Proceedings of the ASME 2016 Dynamic Systems and Control Conference
DSCC 2016
October 12-14, 2016, Minneapolis, USA

DSCC2016-9627

COUPLED OPERATIONAL OPTIMIZATION OF SMART VALVE SYSTEM SUBJECT TO DIFFERENT APPROACH ANGLES OF A PIPE CONTRACTION

Peiman Naseradinmousavi and Mostafa Bagheri
Department of Mechanical Engineering
San Diego State University
San Diego, California

C. Nataraj
Department of Mechanical Engineering
Villanova University
Villanova, Pennsylvania

ABSTRACT

In this paper, we focus on interconnected trajectory optimization of two sets of solenoid actuated butterfly valves dynamically coupled in series. The system undergoes different approach angles of a pipe contraction as a typical profile of the so-called "Smart Valves" network containing tens of actuated valves. A high fidelity interconnected mathematical modeling process is derived to reveal the expected complexity of such a multiphysics system dealing with electromagnetics, fluid mechanics, and nonlinear dynamic effects. A coupled operational optimization scheme is formulated in order to seek the most efficient trajectories of the interconnected valves minimizing the energy consumed enforcing stability and physical constraints. We examine various global optimization methods including Particle Swarm, Simulated Annealing, Genetic, and Gradient based algorithms to avoid being trapped in several possible local minima. The effect of the approach angles of the pipeline contraction on the amount of energy saved is discussed in detail. The results indicate that a substantial amount of energy can be saved by an intelligent operation that uses flow torques to augment the closing efforts.

1 Introduction

Optimization of multi-agent and large-scale electromechanical systems has received much attention due to the potential to reduce energy consumption considerably leading to savings of significant operational and maintenance costs. One of those networks is the flow distribution system being widely used in different applications including municipal piping systems, oil and gas fields, petrochemical plants, and the US Navy chilled water systems [1, 2]. The so-called "Smart Valves" network has received considerable attention to be safely designed and then efficiently operated in critical missions. The main objective of the smart valves is to shut down automatically in case of breakage and to reroute the flow as needed. Optimal design, operation, and control are three main steps of minimizing any system energy consumption with respect to various stability and physical constraints. In this effort, we focus on optimizing the dynamically interconnected valve trajectories in order to reduce the lumped amount of energy consumed in the coupled actuation units.

These sets contain many interdisciplinary components interacting with each other through highly coupled nonlinear dynamics. We have carried out broad analytical and experimental studies from nonlinear modeling to design optimization of both an isolated and interconnected symmetric butterfly valves driven by solenoid actuators [3–11]. The multidisciplinary couplings, including electromagnetics and fluid mechanics, had to be thoroughly considered in the modeling phase in order to yield an accurate nonlinear model of such a complex system. A third-order nondimensional dynamic model of the single set was derived to be used in nonlinear dynamic analysis [5] and optimal design [6].

The dynamic analysis yielded crisis and transient chaotic dynamics of a single actuated valve for some critical physical parameters. A comprehensive stability map was also derived and presented as an efficient tool to determine the safe domain of operation which in turn could serve for identifying the lower and upper bounds for the design optimization efforts. The design optimization was then carried out [6] to select the optimal actuation unit's parameters coupled with the mechanical and fluid parts in

order to significantly reduce the amount of energy consumption (upward of %40).

Note that the applications addressed earlier contain scores of actuated valves in which a high level of dynamic coupling has been observed in practice. These dynamic couplings among different sets need to be captured through analytical studies. We have developed [7] a novel nonlinear model for two sets of solenoid actuated butterfly valves operating in series. The closing/opening valves were modeled as changing resistors and the flow between them as a constant one. A nonlinear coupled model revealed the high dynamic sensitivity of each element of a set, the valve and the actuator, to another one and vice versa. The power spectrum was used in confirming the same frequency response of a neighbor set due to the external periodic noise applied on another set of the valve and actuator.

In further studies, we optimized the design of coupled actuation units of two sets operating in series [10] subject to a sudden contraction. The pipe contraction imposed an additional resistance to be modeled and therefore, the coupled dynamic equations derived in [7] had to be slightly modified (which we represent here for completeness). We discovered an interesting coupling between currents of the actuation units through the interconnected flow loads, including hydrodynamic and bearing torques, which affect the dynamics of both the valves.

Optimization of electromechanical and multidisciplinary systems has recently received much attention. Klimovich [12] obtained some optimal decisions for one-and two-dimensional axisymmetrical flow models. Sefkat [13] has minimized volume and power dissipation by deriving expressions for consumed power, magnetic attraction force, coil temperature and magnet volume, depending on the dimensions. Elka and Bucher [14] discussed the optimal shape design of segmented spatial sensors and actuators that isolate selected mode shapes and perform modal filtering. Raulli and Maute [15] addressed the design of electrostatically actuated microelectromechanical systems by topology optimization such that the layout of the structure and the electrode are simultaneously optimized. Grierson and Pak [16] investigated an approximate design fitness evaluation technique with the aim of improving the numerical efficiency of the genetic search algorithm. Other contributions in operational and design optimization of electromechanical systems include [17–38].

In this paper, the optimal operation process is formulated to help select the appropriate trajectories of the valves coupled with the electromagnetical, mechanical, and fluid parts in order to yield an energy efficient system. The contribution of this work is to optimize both the valves' trajectories dynamically coupled in different aspects while our previous efforts [6, 8, 10] were on optimizing the design of the single (by neglecting its dynamic coupling with another set) and coupled actuation units. In this effort, a lumped cost function will be minimized, while enforcing the stability and physical constraints, using four global optimization tools to avoid being trapped in possible local minima along with the objective of obtaining the most efficient operations of the coupled valves.

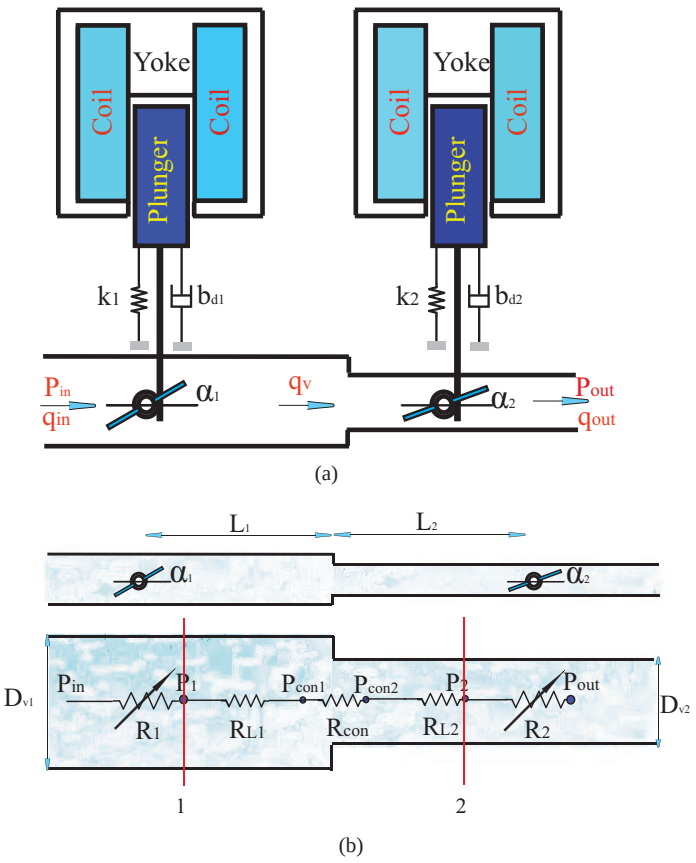

FIGURE 1. (a) A schematic configuration of two solenoid actuated butterfly valves subject to the sudden contraction; (b) A coupled model of two butterfly valves in series without actuation

2 Mathematical Modeling

Shown in Fig. 1(a) is a pair of symmetric butterfly valves driven by solenoid actuators through rack and pinion arrangements. The rack and pinion mechanism provides a kinematic constraint which connects the dynamics of the valve and actuator. Applying DC voltages, as being used in the Navy ships for chilled water systems, the motive forces give translational motions to the actuators' moving parts (plungers) and subsequently the valves rotate to desirable angles. Note that a return spring has been a common practice among industries to open the valves.

Interconnected modeling of such a multiphysics system undoubtedly needs some simplifying assumptions to reduce time consuming numerical calculations. The force resulting from the magnetic field need an extremely short period of time to reach its maximum value. This period is the so-called "Diffusion Time" and has an inverse relationship with the amount of current used.

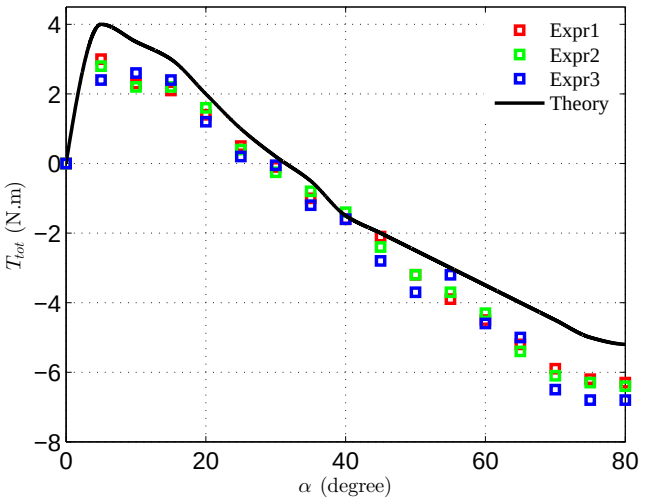

FIGURE 2. A comparison between the experimental and analytical total torques

TABLE 1. The *system* parameters

ρ	$1000\frac{kg}{m^3}$	v	$3\frac{m}{s}$
μ	0.5	P_{in}	256(kPa)
$J_{1,2}$	$0.104\times10^{-1}(kg.m^2)$	$b_{d1,d2}$	$8420\frac{N.m.s}{rad}$
N_1	3300	$C_{11,22}$	$1.56\times10^{6}(H^{-1})$
$g_{m1,m2}$	0.1(m)	$V_{1,2}$	24(Volt)
D_{v1}	0.2032(m)	D_{v2}	0.127(m)
$D_{s1,s2}$	0.01(m)	P_{out}	2(kPa)
$k_{1,2}$	$60(N.m^{-1})$	$C_{21,22}$	$6.32\times10^{8}(H^{-1})$
L_1	2(m)	L_2	1(m)
μ_f	$0.018\ (Kg.m^{-1}.s^{-1})$	$R_{1,2}$	$1(\Omega)$
$r_{1,2}$	0.05(m)	θ	90°
N_2	3300		

Note that using the current of 24 (A) would yield a negligible diffusion time of $\tau_d \approx 2(ms)$ [3] with respect to the nominal operation time of 180(s).

As is commonly done for valve studies, we will assume dominant laminar flow for both the coupled valves to avoid the numerical difficulties involved with a turbulent regime. Note that developing an analytical model is necessary to carry out the dynamic analysis and optimization. Nevertheless, a crucial question needs to be carefully answered with respect to the validity of such an assumption. Using the values of pipe diameter and flow mean velocity listed in Table 1, one can easily distinguish the existence of the turbulent regime which invalidates the assumption we have made. From another aspect, the analytical formulas derived for the flow loads, including the hydrodynamic and bearing torques, have been developed based on the assumption of laminar flow [39, 40]. To address the issues discussed above, we have carried out experimental work to measure the sum of the hydrodynamic and bearing torques as the most affecting loads on the valves and subsequently, the dynamics of the actuators [10]. The experiment yielded the total torque (Fig. 2) for the inlet velocity of $v \approx 2.7\left(\frac{m}{s}\right)$ and valve diameter of $D_v = 2\ (inches)$ reasonably validating the laminar flow assumption [41].

The flow torques have been shown to play a highly important role for the dynamics of an isolated solenoid actuated butterfly valve and we hence expect to observe such effects for the interconnected sets [7] as well. The coupled system is modeled as a set of five resistors. Two changing resistors represent the closing/opening valves, two constant ones indicate head losses between the valves, and fifth is due to the pipe contraction as shown in Fig. 1(b). The inlet and outlet pressures are as shown in Table 1. Using the assumption of the dominant laminar flow, the pressure drops between two valves can be expressed based on the Hagen-Poiseuille [42] and Borda-Carnot [43] formulas (points 1 and 2):

$$P_1 - P_{con1} = \underbrace{\frac{128\mu_f L_1}{\pi D_{v1}^4}}_{R_{L1}} q_v \tag{1}$$

$$P_{con1} - P_{con2} = \frac{1}{2}K_{con}\rho v_{out}^2 \tag{2}$$

$$P_{con2} - P_2 = \underbrace{\frac{128\mu_f L_2}{\pi D_{v2}^4}}_{R_{L2}} q_v \tag{3}$$

where, q_v is the volumetric flow rate, μ_f indicates the fluid dynamic viscosity, D_{v1} and D_{v2} are the valves' diameters, L_1 and L_2 stand for the pipe lengths before and after contraction, R_{L1} and R_{L2} indicate the constant resistances, and P_{con1} and P_{con2} are the flow pressures before and after contraction. K_{con} is calculated as the following:

$$K_{con} = 0.5(1-\beta^2)\sqrt{\sin\left(\frac{\theta}{2}\right)} \tag{4}$$

where, β indicates the ratio of minor and major diameters $\left(\frac{D_{v2}}{D_{v1}}\right)$ and θ is the angle of approach. The values listed in Table 1 easily

yield $K_{con} = 0.2562$. We then rewrite Eq. 2 as follows:

$$\begin{aligned} P_{con1} - P_{con2} &= \frac{1}{2} K_{con} \rho v_{out}^2 \\ &= \underbrace{\frac{8K_{con}}{\pi^2 D_{v2}^4} \rho}_{R_{con}} \underbrace{\frac{\pi^2 D_{v2}^4 v_{out}^2}{16}}_{q_v^2} \\ &= R_{con} q_v^2 \end{aligned} \tag{5}$$

where, R_{con} is the resistance due to the pipe contraction. The pressure drop between the valves can be derived by adding Eqs. 1,2, 3, and 5:

$$P_1 - P_2 = [R_{L1} + R_{L2} + R_{con} q_v] q_v \tag{6}$$

The valve's resistance (R) and coefficient (c_v), being important parameters of the regulating valves, are nonlinear functions of the valve rotation angle and are determined [44] as follows:

$$R_i(\alpha_i) = \frac{891 D_{vi}^4}{c_{vi}^2(\alpha_i)},\ i = 1,2 \tag{7}$$

Based on the assumption of laminar flow, the valve's pressure drop is calculated via the following relationship [39]:

$$\Delta P_i(\alpha_i) = 0.5 R_i(\alpha_i) \rho v^2 \tag{8}$$

where, α indicates the valve rotation angle, ρ is the density of the media, and v stands for the flow velocity. Rewriting Eq. 8 in the standard form yields,

$$\Delta P_i(\alpha_i) = \underbrace{\frac{\pi^2 D_{vi}^4 v^2}{16}}_{q_v^2} \underbrace{\frac{8 \times R_i(\alpha_i) \rho}{\pi^2 D_{vi}^4}}_{R_{ni}(\alpha_i)} = R_{ni}(\alpha_i) q_v^2 \tag{9}$$

The hydrodynamic (T_h) and bearing (T_b) torques [39, 40] are obtained via Eq. 9 leading us to rewrite them as follows.

$$T_{hi} = \frac{16 T_{ci}(\alpha_i) D_{vi}^3 \Delta P_i}{3\pi \left(1 - \frac{C_{cci}(\alpha_i)(1-\sin(\alpha_i))}{2}\right)^2} = f_i(\alpha_i) D_{vi}^3 \Delta P_i \tag{10}$$

$$T_{bi} = 0.5 A_d \Delta P_i \mu D_s = C_i \Delta P_i \tag{11}$$

where, D_s stands for the stem diameter of the valve, μ indicates the friction coefficient of the bearing area, $C_i = \frac{\pi}{8} \mu D_{vi}^2 D_s$, and T_{ci} and C_{cci} are the hydrodynamic torque and the sum of upper and lower contraction coefficients, respectively, depending on the valve rotation angle [3]. Further,

$$f_i(\alpha_i) = \frac{16 T_{ci}(\alpha_i)}{3\pi \left(1 - \frac{C_{cci}(\alpha_i)(1-\sin(\alpha_i))}{2}\right)^2} \tag{12}$$

The comprehensive stability map we have presented in [5] was based on a nonlinear analytical model. The analytical model had to be used in the dynamic analysis to investigate the system stability around equilibria by calculating its eigenvalues through the Jacobian matrix; this has led us to identify the safe operational domain to be utilized in the design optimization. The same practice was employed in [10] with the aid of fitting suitable curves on c_{vi} and R_{ni} in order to model the system analytically. For our case study of D_{v1}=8 (in) and D_{v2}=5 (in), the coefficients and resistances of the valves are developed as follows.

$$c_{v1}(\alpha_1) = p_1 \alpha_1^3 + q_1 \alpha_1^2 + o_1 \alpha_1 + s_1 \tag{13}$$

$$c_{v2}(\alpha_2) = p_2 \alpha_2^3 + q_2 \alpha_2^2 + o_2 \alpha_2 + s_2 \tag{14}$$

$$R_{n1}(\alpha_1) = \frac{e_1}{(p_1 \alpha_1^3 + q_1 \alpha_1^2 + o_1 \alpha_1 + s_1)^2} \tag{15}$$

$$R_{n2}(\alpha_2) = \frac{e_2}{(p_2 \alpha_2^3 + q_2 \alpha_2^2 + o_2 \alpha_2 + s_2)^2} \tag{16}$$

where, $e_1 = 7.2 \times 10^5$, $p_1 = 461.9$, $q_1 = -405.4$, $o_1 = -1831$, $s_1 = 2207$, $e_2 = 4.51 \times 10^5$, $p_2 = 161.84$, $q_2 = -110.53$, $o_2 = -695.1$, and $s_2 = 807.57$. These fittings were selected with respect to the decremental and incremental profiles of the valve coefficients and resistances, respectively [7, 41]. Applying the mass continuity principle ($q_{in} = q_{out} = q_v$) and then rewriting Eq. 9 yields,

$$\frac{P_{in} - P_1}{R_{n1}(\alpha_1)} = \frac{P_2 - P_{out}}{R_{n2}(\alpha_2)} \tag{17}$$

$$R_{n1} P_2 + R_{n2} P_1 = R_{n2} P_{in} + R_{n1} P_{out} \tag{18}$$

The interconnected P_1 and P_2 terms are derived by combining Eqs. 6 and 18 as follows:

$$P_1 = \frac{R_{n2} P_{in} + R_{n1} P_{out} + R_{n1}(R_{L1} + R_{L2} + R_{con} q_v) q_v}{(R_{n1} + R_{n2})} \tag{19}$$

$$P_2 = \frac{R_{n2} P_{in} + R_{n1} P_{out} - R_{n2}(R_{L1} + R_{L2} + R_{con} q_v) q_v}{(R_{n1} + R_{n2})} \tag{20}$$

The dynamic sensitivities of P_1 and P_2 to R_{n1}, R_{n2}, R_{L1}, R_{L2}, and R_{con} are distinguishable through Eqs. 19 and 20. Any slight dynamic changes of the upstream set of the valve-actuator would be expected to be observed for the downstream one, in fact, as often observed in practice. The dependencies of the hydrodynamic and bearing torques on all the resistances are reformulated as follows.

$$T_{hi} = f_i(\alpha_i) D_{vi}^3 \Delta P_i(R_{n1}, R_{n2}, R_{L1}, R_{L2}, R_{con}) \tag{21}$$

$$T_{bi} = C_i \Delta P_i(R_{n1}, R_{n2}, R_{L1}, R_{L2}, R_{con}) \tag{22}$$

f_i is a nonlinear function of the changing T_{ci}, C_{cci}, and the valve rotation angles. To carry out a systematic dynamic analysis, the following functions are fitted to the $D_{vi}^3 f_i$ of each valve [7, 41]:

$$\begin{aligned} T_{h1} &= \underbrace{(a_1\alpha_1 e^{b_1{\alpha_1}^{1.1}} - c_1 e^{d_1\alpha_1})}_{D_{v1}^3 f_1}(P_{in} - P_1) \\ &= (a_1\alpha_1 e^{b_1{\alpha_1}^{1.1}} - c_1 e^{d_1\alpha_1}) \times \frac{\frac{e_1}{(p_1\alpha_1^3 + q_1\alpha_1^2 + o_1\alpha_1 + s_1)^2}}{\sum_{i=1}^{2} \frac{e_i}{(p_i\alpha_i^3 + q_i\alpha_i^2 + o_i\alpha_i + s_i)^2}} \\ &\times (P_{in} - P_{out} - (R_{L1} + R_{L2} + R_{con}q_v)q_v) \end{aligned} \tag{23}$$

$$\begin{aligned} T_{h2} &= \underbrace{(a_1'\alpha_2 e^{b_1'{\alpha_2}^{1.1}} - c_1' e^{d_1'\alpha_2})}_{D_{v2}^3 f_2}(P_2 - P_{out}) \\ &= (a_1'\alpha_2 e^{b_1'{\alpha_2}^{1.1}} - c_1' e^{d_1'\alpha_2}) \times \frac{\frac{e_2}{(p_2\alpha_2^3 + q_2\alpha_2^2 + o_2\alpha_2 + s_2)^2}}{\sum_{i=1}^{2} \frac{e_i}{(p_i\alpha_i^3 + q_i\alpha_i^2 + o_i\alpha_i + s_i)^2}} \\ &\times (P_{in} - P_{out} - (R_{L1} + R_{L2} + R_{con}q_v)q_v) \end{aligned} \tag{24}$$

where, $a_1 = 0.4249$, $a_1' = 0.1022$, $b_1 = -18.52$, $b_1' = -17.0795$, $c_1 = -7.823 \times 10^{-4}$, $c_1' = -2 \times 10^{-4}$, $d_1 = -1.084$, and $d_1' = -1.0973$.

We have previously derived the rate of current and magnetic force terms [3] which are utilized in developing the sixth-order coupled dynamic model [10] as follows. Note that both the motive force and current are highly sensitive to the plunger displacement and subsequently the valve rotation angle.

$$F_{mi} = \frac{C_{2i} N_i^2 i_i^2}{2(C_{1i} + C_{2i}(g_{mi} - x_i))^2} \tag{25}$$

$$\frac{di_i}{dt} = \frac{(V_i - R_i i_i)(C_{1i} + C_{2i}(g_{mi} - x_i))}{N_i^2} - \frac{C_{2i} i_i \dot{x}_i}{(C_{1i} + C_{2i}(g_{mi} - x_i))} \tag{26}$$

$$\dot{z}_1 = z_2 \tag{27}$$

$$\begin{aligned} \dot{z}_2 = \frac{1}{J_1} \Bigg[&\frac{r_1 C_{21} N_1^2 z_3^2}{2(C_{11} + C_{21}(g_{m1} - r_1 z_1))^2} - b_{d1} z_2 - k_1 z_1 \\ &+ \frac{\frac{(P_{in} - P_{out} - (R_{L1} + R_{L2} + R_{con}q_v)q_v)e_1}{(p_1 z_1^3 + q_1 z_1^2 + o_1 z_1 + s_1)^2}}{\sum_{i=1,4} \frac{e_i}{(p_i z_i^3 + q_i z_i^2 + o_i z_i + s_i)^2}} \times \\ &\Big[(a_1 z_1 e^{b_1 {z_1}^{1.1}} - c_1 e^{d_1 z_1}) - C_1 \times \tanh(K z_2) \Big] \Bigg] \end{aligned} \tag{28}$$

$$\dot{z}_3 = \frac{(V_1 - R_1 z_3)(C_{11} + C_{21}(g_{m1} - r_1 z_1))}{N_1^2} - \frac{r_1 C_{21} z_3 z_2}{(C_{11} + C_{21}(g_{m1} - r_1 z_1))} \tag{29}$$

$$\dot{z}_4 = z_5 \tag{30}$$

$$\begin{aligned} \dot{z}_5 = \frac{1}{J_2} \Bigg[&\frac{r_2 C_{22} N_2^2 z_6^2}{2(C_{12} + C_{22}(g_{m2} - r_2 z_4))^2} - b_{d2} z_5 - k_2 z_4 \\ &+ \frac{\frac{(P_{in} - P_{out} - (R_{L1} + R_{L2} + R_{con}q_v)q_v)e_2}{(p_2 z_4^3 + q_2 z_4^2 + o_2 z_4 + s_2)^2}}{\sum_{i=1,4} \frac{e_i}{(p_i z_i^3 + q_i z_i^2 + o_i z_i + s_i)^2}} \times \\ &\Big[(a_1' z_4 e^{b_1' {z_4}^{1.1}} - c_1' e^{d_1' z_4}) - C_2 \times \tanh(K z_5) \Big] \Bigg] \end{aligned} \tag{31}$$

$$\dot{z}_6 = \frac{(V_2 - R_2 z_6)(C_{12} + C_{22}(g_{m2} - r_2 z_4))}{N_2^2} - \frac{r_2 C_{22} z_5 z_6}{(C_{12} + C_{22}(g_{m2} - r_2 z_4))} \tag{32}$$

where, b_d indicates the equivalent torsional damping, K_t is the equivalent torsional stiffness, V stands for the supply voltage, x is the plunger displacement, r indicates the radius of the pinion, C_1 and C_2 are the reluctances of the magnetic path without air gap and that of the air gap, respectively, F_m is the motive force, N stands for the number of coils, i indicates the applied current, g_m is the nominal airgap, J indicates the polar moment of inertia of the valve's disk, and R is the electrical resistance of coil.

3 Optimal Operation

The stability and physical constraints reported in [4, 5] undoubtedly demand robust optimization schemes to be utilized in minimizing the energy consumed by two coupled sets. Note that operating the system without the constraints determined through the nonlinear dynamic analysis would undesirably lead to the

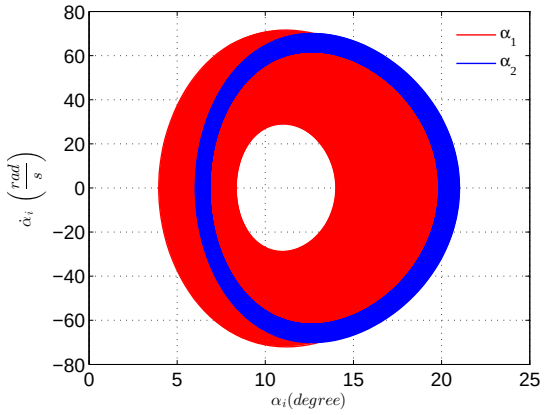

(a)

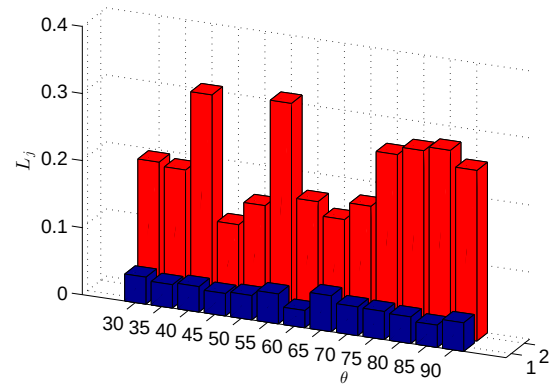

(b)

FIGURE 3. (a) Chaotic dynamics of the valves/actuators; (b) Two positive Lyapunov exponents spectra vs. the approach angle indicating the hyperchaotic dynamics of the system

catastrophic failure of the network shown in Fig. 3(a) revealing the hyperchaotic dynamics of both the actuated valves. It can in fact be shown that some critical values of the equivalent viscous damping and friction coefficient of the bearing area ($\mu_i = b_{di} = 10^{-6}$) yield the hyperchaotic dynamics.

The problem at hand is a constrained optimization problem with possibly several local minima. Therefore, we have to employ robust optimization algorithms to capture the global minimum. The cost function we wish to minimize is a sum of the energy used in both the sets.

$$\min E_{tot} = \sum_{i=1}^{2} \int_0^{t_f} Vi_i\, dt \tag{33}$$

subject to:$z_1 < 90^\circ$, $z_4 < 90^\circ$

& Coupled Dynamic Equations

The cost function is typically defined with respect to the scale and performance of the network. Scores of such actuated valves are employed in the US Navy fleet and a minimum lumped amount of energy consumed in the network is needed to reduce the cost of operation. This would lead us to select a lumped cost function to be minimized. We then fit two nonlinear curves to the nominal valve trajectories obtained via Eqs. 27-32:

$$\alpha_1(t) = A\tanh(Bt^4) \tag{34}$$
$$\alpha_2(t) = C\tanh(Dt^4) \tag{35}$$

The nominal values of A, B, C, and D are listed in Table 2. The curves fitted to the nominal trajectories are selected based on desirable smooth valve rotations. The so-called "S-Shaped" valves' motions have traditionally been appropriate trajectories to avoid dangerous behaviors such as the well-known water hammering, in particular, for such critical applications addressed earlier. A, B, C, and D are variables that we need to optimize in order to identify the most efficient valve trajectories yielding minimum energy consumption by using the DC voltage sources ($V_1 = V_2 = 24(Volts)$). Note that $\alpha_1(t)$ and $\alpha_2(t)$ are coupled angles through the interconnected dynamic equations. We next collect the coefficients into a vector:

$$\theta_1 = [A, B, C, D]^T \tag{36}$$

The coupled equations, as discussed earlier, need to be satisfied at all times during the optimization process and the coefficients are subject to the following lower and upper bounds.

$$\theta_{1min} = [0.85, 9.50 \times 10^{-5}, 0.98, 5.99 \times 10^{-5}]^T \tag{37}$$
$$\theta_{1max} = [0.8, 0.1 \times 10^{-7}, 0.92, 0.1 \times 10^{-7}]^T \tag{38}$$

These bounds were determined based on practical system considerations, stability analysis [5, 41], and physical constraints. We employ four global optimization tools including simulated annealing, genetic, particle swarm, and gradient based algorithms to provide a clear map of optimization efforts with respect to the locality/globality of the cost function minima. Simulated annealing was independently developed by Kirkpatrick *et al.* [45] and by Cerny [46]. Genetic optimization has been designed based on a heuristic search to mimic the process of natural selection [47].

The coefficients in practice are not of the same order, and caused serious numerical errors in our initial studies. We solved this issue by conditioning them using a normalization scheme as follows.

$$A_n = A \times 10^3; B_n = B \times 10^7$$
$$C_n = C \times 10^3; D_n = D \times 10^7$$

One of the advantages of the simulated annealing procedure is to select a new point randomly. We hence need to set the initial guesses as random numbers. The algorithm covers all new points to reduce the value of the objective function. At the same time, with a certain probability, points that increase the objective function are also accepted. The algorithm avoids being trapped in local minima by using points that raise the objective function value and has the potential to search globally for more possible solutions.

The genetic algorithm is significantly more robust than other conventional ones. It does not break down easily in the presence of slight changes of inputs, and noise. For a large state-space, the algorithm may potentially exhibit significantly better performance than typical optimization techniques.

The particle swarm optimization (PSO) was originally developed by Kennedy, Eberhart and Shi [48,49] and was first used in simulating social behaviour. PSO is metaheuristic as it makes few or no assumptions about the problem being optimized and can search very large spaces of candidate solutions.

The random initial guesses we used in the optimization process (as required by simulated annealing) are as follows.

$$\theta_{nr} = \theta_{lb} + (\theta_{ub} - \theta_{lb}) \times \text{rand}(0,1) \tag{39}$$

where rand(0,1) is a random number between zero and one. We developed the algorithm in MATLAB.

4 Results

Table 1 contains the parameters obtained from the experimental work we carried out for the isolated set [10]. Figures 4 and 5 reveal the optimization process for the coefficients of curves fitted to the valve angles using the genetic (GA), gradient based (GB), simulated annealing (SA), and particle swarm (PS) algorithms. The GB, GA, SA, and PS algorithms terminate after 4200, 1100, 11500, and 1000 iterations, respectively, satisfying the tolerances defined for both the variables and the lumped cost function. It is of great interest to observe that all methods result in lower values of B, C, and D with respect to their corresponding nominal values listed in Table 2, which in turn would yield slower responses of both the valves than those of the nominal ones. The GB and SA methods lead to lower values of A but the GA and PS yield slightly higher values in comparison with the nominal ones.

Such optimal motions would lead to considerably lower values of the currents of both the actuation units in comparison with the nominal ones, particularly for the downstream set as shown in Figs. 6 and 7. A sudden current drop is distinguishable for the downstream actuator (Fig. 7) at t=34(s). The physical interpretation of such lower values of the currents can be found through the flow dynamics (loads) interconnected with the electromagnetic parts. We have previously established [10] that the change

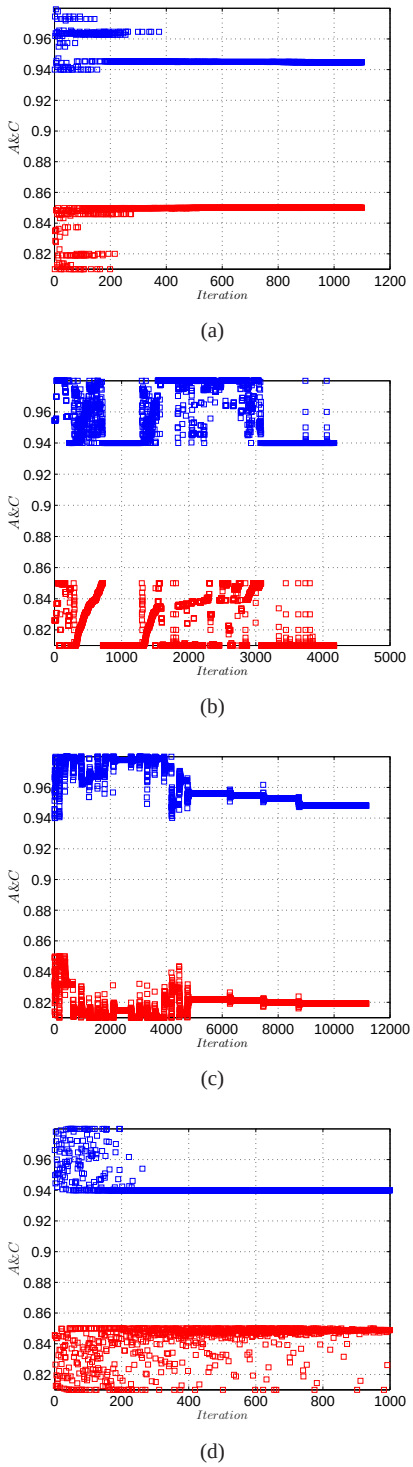

FIGURE 4. The optimized A and C: red and blue squares stand for A and C, respectively; (a) GA; (b) GB; (c) SA; (d) PS

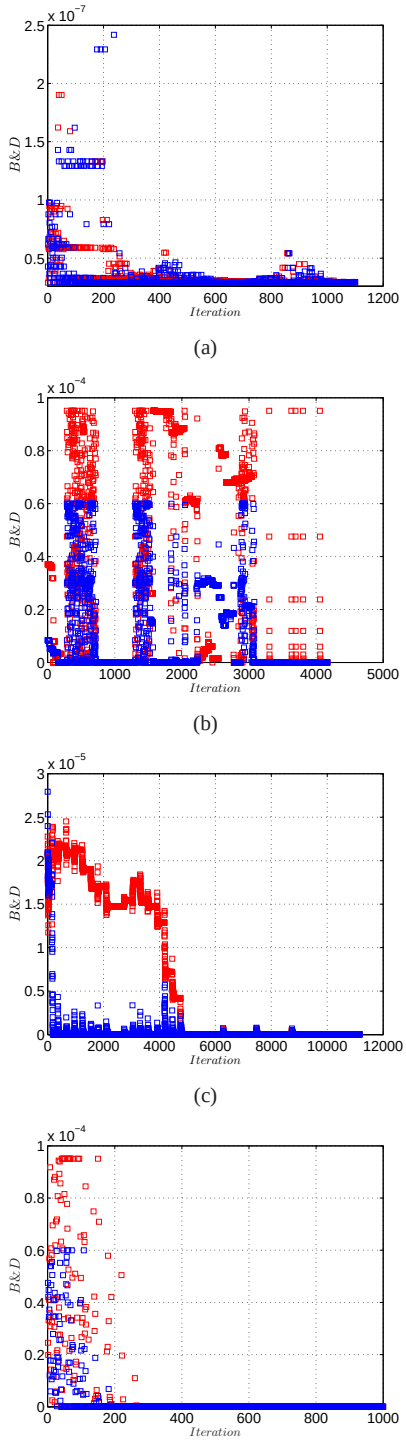

FIGURE 5. The optimized B and D: red and blue squares stand for B and D, respectively; (a) GA; (b) GB; (c) SA; (d) PS

TABLE 2. The nominal and optimal variables

	Nominal	GB	GA	SA	PS
A	0.83	0.81	0.849	0.819	0.8458
$B \times 10^7$	1	0.2911	0.29	0.29	0.29
C	0.95	0.94	0.9448	0.9481	0.94
$D \times 10^7$	1	0.29	0.2924	0.29	0.29
Energy (J)	206880	176900	177930	177680	176890

of pipe diameter would potentially yield higher values of the hydrodynamic torque acting on the downstream valve than that of the upstream one, based on Eqs. 7-9, and 21.

$$\frac{T_{h2}}{T_{h1}} \propto \left(\frac{D_{v2}}{D_{v1}}\right)^3 \times \left(\frac{c_{v1}}{c_{v2}}\right)^2 \tag{40}$$

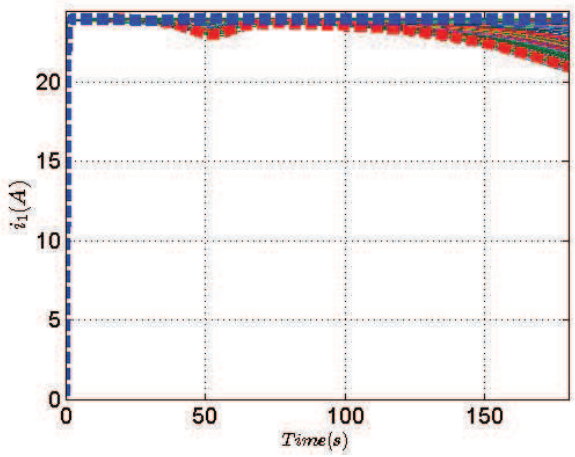

FIGURE 6. The optimal (dashed red line) and nominal (dashed blue line) applied currents of the upstream set

The downstream valve is logically expected, for both the nominal and optimal cases, to be subject to the higher hydrodynamic torque [6] as shown in Fig. 8. We have also discussed the highly important role of the hydrodynamic torque on the valves' operations. The hydrodynamic torque acts as a helping load pushing the valve to be closed and is typically effective for when the valve angle is lower than 60° [7, 10]; the effective range was experimentally examined [7] confirming the helping behavior of the hydrodynamic torque by presenting positive values. Consequently, the higher helping torques would result in the

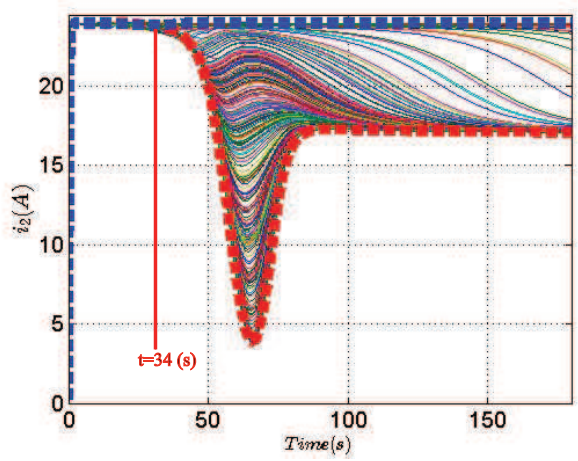

FIGURE 7. The optimal (dashed red line) and nominal (dashed blue line) applied currents of the downstream set

downstream valve's higher rotation angles than those of the upstream ones (for both the nominal and optimal configurations), as shown in Fig. 9; $\alpha_{1no} = 47^\circ$, $\alpha_{2no} = 52.9^\circ$, $\alpha_{1op} = 48^\circ$, and $\alpha_{2op} = 52.73^\circ$.

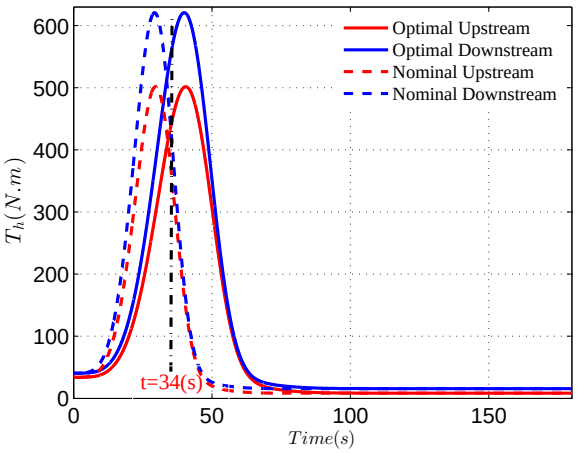

FIGURE 8. The hydrodynamic torque acting on both the valves

Note that Fig. 9 presents the valves' relatively slower motions for the optimal operations in comparison with the nominal ones. These kinds of operationally optimized rotations expose both the coupled valves to the higher hydrodynamic torques (as helping factors) in comparison with the nominal loads, as shown in Fig. 8. This is explicitly distinguishable at t=34(s) by showing the higher hydrodynamic torques afterward and the actuators have subsequently more freedom to act with significantly lower currents, in particular, for the downstream set as it undergoes the higher hydrodynamic load. The optimal motions would lead us

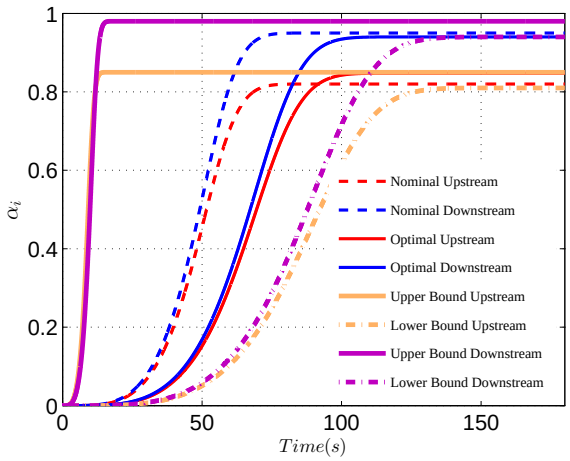

FIGURE 9. The optimal and nominal valves' rotation angles including lower and upper bounds

to consume a lower amount of energy as presented in Fig. 10.

The decreased amounts of energies are spent as shown in Figs. 10(a), 10(b), 10(c), and 10(d). Shown in Figs. 10(a), 10(b), 10(c), and 10(d) indicate 14%, 14.5%, 14.1%, and 14.5% energy savings through the GA, GB, SA, and PS algorithms, respectively. The four optimization schemes were repeatedly examined to avoid being trapped in probable local minima. The negligible difference (less than 0.58%) among the GA, GB, SA, and PS methods would potentially indicate the global minimum value.

It is also of great interest to evaluate the effect of approach angle (θ) on the amount of energy saved. Figure 11 presents an interesting aspect of the optimization problem in that the lumped amount of energy saved for both the sets is higher for a smaller approach angle in comparison with a higher value. The physical interpretation of such an energy consumption paradigm can be found through Eqs. 19 and 20. The higher approach angle yields the higher contraction resistance (R_{con}), lower P_2, and subsequently lower pressure drop across the downstream valve. Note that the downstream set has a higher share in minimizing the energy consumption by experiencing the sudden current drop (Fig. 7). The lower pressure drop of the downstream valve would result in the lower value of the helping hydrodynamic torque as previously explained via Eq. 21. The actuation unit of the downstream set located after a sharper pipe contraction (a large value of θ) has therefore less freedom to save the lumped energy than that of a smoother contraction.

5 Conclusions and Future Work

In this paper, we represented a novel interconnected nonlinear model of two solenoid actuated valves subject to the different approach angles of the pipeline contraction. We revealed the significant effects of mutual interactions between the dynamics of the valves and the actuators in correlations with the flow non-

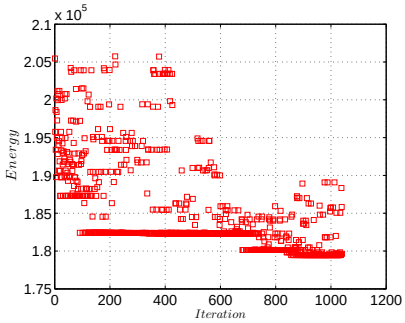

(a)

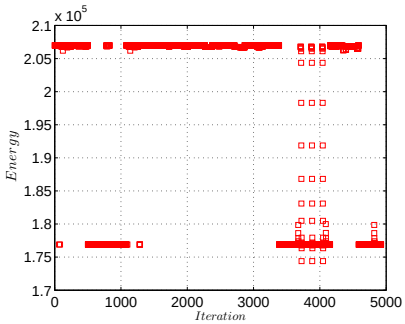

(b)

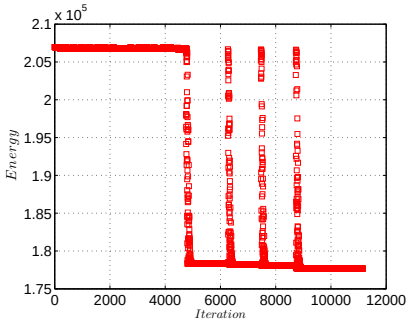

(c)

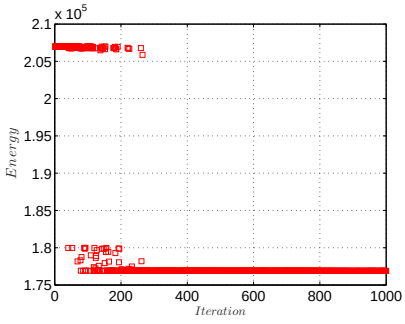

(d)

FIGURE 10. The optimized lumped amount of energy: (a) GA ($E_{opm} = 177930$); (b) GB ($E_{opm} = 176900$); (c) SA ($E_{opm} = 177680$); (d) PS ($E_{opm} = 176890$)

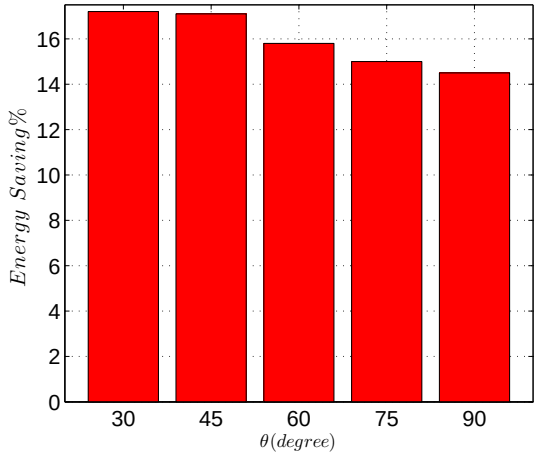

FIGURE 11. The amount of saved energy vs. the approach angle

linear torques. These couplings among different elements were accurately formalized to derive a sixth order dynamic model of the whole system. We utilized particle swarm, genetic, simulated annealing, and gradient based schemes to carry out operational optimization and subsequently captured the global minimum of the lumped cost function defined as the sum of energy used in each set.

The principal results of this paper can be summarized as follows.

- The approach angle has an inverse relationship with the amount of energy saved for both the sets. The sharper pipe contraction yields the higher value of energy consumption.
- Energy can be saved by significant amounts of 17.2%, 17%, 16%, 15%, and 15% for the approach angles of 30°, 45°, 60°, 75°, and 90°, respectively, by using operationally optimized coupled valves.
- The optimal hydrodynamic torques help actuators spend a minimum level of the lumped energy.
- Lower values of the currents and subsequently instantaneous energies (by plotting $E_{ins} = v_i i_i$ vs. α_i) are consumed particularly for higher rotation angles.

We are currently focusing our efforts on developing a comprehensive model for n valves and actuators to be operated optimally in series.

ACKNOWLEDGMENT

The experimental work of this research was supported by Office of Naval Research Grant (N00014/2008/1/0435). We greatly appreciate this grant and the advice and direction provided by Mr. Anthony Seman III, the program manager.

REFERENCES

[1] Hughes, R., Balestrini, S., Kelly, K., Weston, N., and Mavris, D., 2006. "Modeling of an integrated reconfigurable intelligent system (IRIS) for ship design". In Proceedings of the 2006 ASNE Ship and Ship Systems Technology (S3T) Symposium.

[2] Lequesne, B., Henry, R., and Kamal, M., 1998. Magnavalve: a new solenoid configuration based on a spring-mass oscillatory system for engine valve actuation. GM Research Report E3-89, June.

[3] Naseradinmousavi, P., and Nataraj, C., 2011. "Nonlinear mathematical modeling of butterfly valves driven by solenoid actuators". *Journal of Applied Mathematical Modelling*, **35**(5), pp. 2324–2335.

[4] Naseradinmousavi, P., and Nataraj, C., 2011. "A chaotic blue sky catastrophe of butterfly valves driven by solenoid actuators". In Proceedings of the ASME 2011 International Mechanical Engineering Congress & Exposition, Vol. 7: Dynamic Systems and Control; Mechatronics and Intelligent Machines, Parts A and B, pp. 25–31.

[5] Naseradinmousavi, P., and Nataraj, C., 2012. "Transient chaos and crisis phenomena in butterfly valves driven by solenoid actuators". *Communications in Nonlinear Science and Numerical Simulation*, **17**(11), November, pp. 4336–4345.

[6] Naseradinmousavi, P., and Nataraj, C., 2013. "Optimal design of solenoid actuators driving butterfly valves". *ASME Journal of Mechanical Design*, **135**(9), July.

[7] Naseradinmousavi, P., 2015. "A novel nonlinear modeling and dynamic analysis of solenoid actuated butterfly valves coupled in series". *ASME Journal of Dynamic Systems, Measurement, and Control*, **137**(1), January.

[8] Naseradinmousavi, P., and Nataraj, C., 2015. "Design optimization of solenoid actuated butterfly valves dynamically coupled in series". In Proceedings of the ASME 2015 Dynamic Systems and Control Conference, Vol. 2: Diagnostics and Detection; Drilling; Dynamics and Control of Wind Energy Systems; Energy Harvesting; Estimation and Identification; Flexible and Smart Structure Control; Fuels Cells/Energy Storage; Human Robot Interaction; HVAC Building Energy Management; Industrial Applications; Intelligent Transportation Systems; Manufacturing; Mechatronics; Modelling and Validation; Motion and Vibration Control Applications, p. V002T33A001.

[9] Naseradinmousavi, P., 2015. "Optimal design of solenoid actuated butterfly valves dynamically coupled in series". In Proceedings of the ASME 2015 International Mechanical Engineering Congress & Exposition, Vol. 4A: Dynamics, Vibration, and Control, p. V04AT04A032.

[10] Naseradinmousavi, P., Krstic, M., and Nataraj, C., 2016. "Design optimization of dynamically coupled actuated butterfly valves subject to a sudden contraction". *ASME Journal of Mechanical Design*, **138**(4), April, p. 041402.

[11] Naseradinmousavi, P., Segala, D. B., and Nataraj, C., 2016. "Chaotic and hyperchaotic dynamics of smart valves system subject to a sudden contraction". *Journal of Computational and Nonlinear Dynamics*, **11**(5), September, p. 051025.

[12] Klimovich, V. I., 1997. "On the optimal design of the form of hydroturbine impeller blades". *Structural and Multidisciplinary Optimization*, **13**(1), February, pp. 29–35.

[13] Sefkat, G., 2009. "The design optimization of the electromechanical actuator". *Structural and Multidisciplinary Optimization*, **37**(6), pp. 635–644.

[14] Elka, A., and Bucher, I., 2009. "Optimal electrode shaping for precise modal electromechanical filtering". *Structural and Multidisciplinary Optimization*, **38**(6), July, pp. 627–641.

[15] Raulli, M., and Maute, K., 2005. "Topology optimization of electrostatically actuated microsystems". *Structural and Multidisciplinary Optimization*, **30**(5), November, pp. 342–359.

[16] Grierson, D. E., and Pak, W. H., 1993. "Optimal sizing, geometrical and topological design using a genetic algorithm". *Structural and Multidisciplinary Optimization*, **6**(3), September, pp. 151–159.

[17] Marquardt, D., 1963. "An algorithm for least-squares estimation of nonlinear parameters". *SIAM Journal Applied Math.*, **11**, pp. 431–441.

[18] Bittanti, S., Fronza, G., and Guardabassi, G., 1976. "Optimal steady-state versus periodic operation in discrete systems". *Journal of Optimization Theory and Applications*, **18**(4), April, pp. 521–536.

[19] Abdel-Halim, M. A., Christensen, G. S., and Kelly, D. H., 1985. "Optimal load frequency control with governor backlash". *Journal of Optimization Theory and Applications*, **45**(4), April, pp. 505–516.

[20] Soliman, S. A., Christensen, G. S., and Abdel-Halim, M. A., 1986. "Optimal operation of multireservoir power systems". *Journal of Optimization Theory and Applications*, **49**(3), pp. 449–461.

[21] Lee, K., Ortiz, J. L., Mohtadi, M. A., and Park, Y. M., 1988. "Optimal operation of large-scale power systems". *IEEE Transactions on Power Systems*, **3**(2), pp. 413–420.

[22] Christensen, G. S., and Soliman, S. A., 1989. "Long-term optimal operation of series parallel reservoirs for critical period with specified monthly generation and average monthly storage". *Journal of Optimization Theory and Applications*, **63**(3), December, pp. 333–353.

[23] Ulanicki, B., and Orr, C. H., 1991. "Unified approach for the optimization of nonlinear hydraulic systems". *Journal of Optimization Theory and Applications*, **68**(1), January, pp. 161–179.

[24] Stern, H. I., 1992. "Optimal control of a facility with peri-

odic interrupted demand". *Journal of Optimization Theory and Applications*, **73**(3), June, pp. 577–599.
[25] Mezyk, A., 1994. "Minimization of transient forces in an electro-mechanical system". *Structural and Multidisciplinary Optimization*, **8**(4), December, pp. 251–256.
[26] Yu, G., Powell, R. S., and Sterling, M. J. H., 1994. "Optimized pump scheduling in water distribution systems". *Journal of Optimization Theory and Applications*, **83**(3), December, pp. 463–488.
[27] Kajima, T., 1995. "Dynamic model of the plunger type solenoids at deenergizing state". *IEEE Transactions on Magnetics*, **31**(3), May, pp. 2315 – 2323.
[28] Messine, F., Nogarede, B., , and Lagouanelle, J. L., 1998. "Optimal design of electromechanical actuators: A new method based on global optimization". *IEEE TRANSACTIONS ON MAGNETICS*, **34**(1), pp. 299–308.
[29] Kelley, C. T., 1999. "Iterative methods for optimization". *Frontiers in Applied Mathematics*, **18**.
[30] Sung, B. J., Lee, E. W., and Kim, H. E., 2002. "Development of design program for on and off type solenoid actuator". In Proceedings of the KIEE Summer Annual Conference, Vol. B, pp. 929–931.
[31] Karr, C. L., and Scott, D. A., 2003. "Genetic algorithm frequency domain optimization of an anti-resonant electromechanical controller". *Lecture Notes in Computer Science*.
[32] Baek-Ju, S., and Eun-Woong, L., 2005. "Optimal design and speed increasing method of solenoid actuator using a non-magnetic ring". In International Conference on Power Electronics and Drives Systems, pp. 1140 – 1145.
[33] Zhao, L., and Chai, T., 2005. *Wastewater BOD Forecasting Model for Optimal Operation Using Robust Time-Delay Neural Network*, Vol. 3498. Springer Berlin Heidelberg, ch. Advances in Neural Networks-ISNN 2005, pp. 1028–1033.
[34] Nowak, L., 2010. "Optimization of the electromechanical systems on the basis of coupled field-circuit approach". *The international journal for computation and mathematics in electrical and electronic engineering*, **20**(1), pp. 39–52.
[35] Engell, S., and Harjunkoski, I., 2012. "Optimal operation: Scheduling, advanced control and their integration". *Computers and Chemical Engineering*, **47**, December, pp. 121–133.
[36] Abergel, J., Allain, M., Michaud, H., Cueff, M., Ricart, T., Dieppedale, C., Rhun, G. L., Faralli, D., Fanget, S., and Defay, E., 2012. "Optimized gradient-free pzt thin films for micro-actuators". In 2012 IEEE International Ultrasonics Symposium (IUS), IEEE.
[37] Bonami, P., Olivares, A., and Staffetti, E., 2014. "Energy-optimal multi-goal motion planning for planar robot manipulators". *Journal of Optimization Theory and Applications*, **163**(1), 80-104.
[38] Mahdi, S. A., 2014. "Optimization of pid controller parameters based on genetic algorithm for non-linear electromechanical actuator". *International Journal of Computer Applications*, **94**, November.
[39] Park, J. Y., and Chung, M. K., 2006. "Study on hydrodynamic torque of a butterfly valve". *Journal of Fluids Engineering*, **128**(1), January, pp. 190–195.
[40] Leutwyler, Z., and Dalton, C., 2008. "A CFD study of the flow field, resultant force, and aerodynamic torque on a symmetric disk butterfly valve in a compressible fluid". *Journal of Pressure Vessel Technology*, **130**(2).
[41] Naseradinmousavi, P., 2012. "Nonlinear modeling, dynamic analysis, and optimal design and operation of electromechanical valve systems". PhD thesis, Villanova University, May.
[42] Bennett, C. O., and Myers, J. E., 1962. *Momentum, heat, and mass transfer*. McGraw-Hill.
[43] Massey, B. S., and Ward-Smith, J., 1998. *Mechanics of Fluids*, 7th ed. Taylor & Francis.
[44] Association, A. W. W., 2012. *Butterfly Valves: Torque, Head Loss, and Cavitation Analysis*, 2nd ed.
[45] Kirkpatrick, S., Gelatt, C. D., and Vecchi, M. P., 1983. "Optimization by simulated annealing". *Science*, **220**(4598), pp. 671–680.
[46] Cerny, V., 1985. "Thermodynamical approach to the traveling salesman problem: An efficient simulation algorithm". *Journal of Optimization Theory and Applications*, **45**(1), January, pp. 41–55.
[47] H., H. J., 1975. *Adaptation in Natural and Artificial Systems*. Adaptation in Natural and Artificial Systems.
[48] Kennedy, J., and Eberhart, R., 1995. "Particle swarm optimization". In Proceedings of IEEE International Conference on Neural Networks, pp. 1942–1948.
[49] Shi, Y., and Eberhart, R. C., 1998. "A modified particle swarm optimizer". In Proceedings of IEEE International Conference on Evolutionary Computation, pp. 69–73.